Maximum-Likelihood Synchronization and Channel Estimation for OFDMA Uplink Transmissions

Man-On Pun, *Student Member, IEEE*, Michele Morelli, *Member, IEEE*, and C.-C. Jay Kuo, *Fellow, IEEE*

Abstract—Maximum-likelihood estimation of the carrier frequency offset (CFO), timing error, and channel response of each active user in the uplink of an orthogonal frequency-division multiple-access system is investigated in this study, assuming that a training sequence is available. The exact solution to this problem turns out to be too complex for practical purposes as it involves a search over a multidimensional domain. However, making use of the alternating projection method, we replace the above search with a sequence of mono-dimensional searches. This results in an estimation algorithm of a reasonable complexity which is suitable for practical applications. As compared with other existing semi-blind methods, the proposed algorithm requires increased overhead but has more flexibility as it can be used with any subcarrier assignment scheme. Simulations indicate that the accuracy of the CFO estimates asymptotically achieves the Cramer–Rao bound.

Index Terms—Channel estimation, frequency synchronization, orthogonal frequency-division multiple access (OFDMA), timing synchronization.

I. INTRODUCTION

ORTHOGONAL frequency-division multiple access (OFDMA) has attracted much attention in the last years since it is widely recognized as a promising technique for fourth-generation (4G) broadband wireless networks [1]. In an OFDMA system, several users simultaneously transmit their own data by modulating an exclusive set of orthogonal subcarriers. Two critical issues in OFDMA uplink transmissions are: frequency/timing synchronization and channel estimation. Similar to orthogonal frequency-division multiplexing (OFDM), OFDMA is particularly sensitive to carrier frequency offsets (CFOs) and timing errors. Inaccurate CFO estimation produces intercarrier interference (ICI) due to the loss of orthogonality among subcarriers. Timing errors result in interblock interference (IBI) between adjacent OFDMA blocks and must be counteracted to avoid severe error rate degradation.

In quasi-synchronous multiple-access systems, the user's timing is locked to a signal received from the base station (BS) through a downlink synchronization channel. As a consequence, timing offsets in the uplink are mainly due to the propagation delay incurred by users' signals. Depending on the cell radius, they can be limited to a few sampling intervals and incorporated as part of the unknown channel impulse response (CIR). Under such a circumstance, the use of a sufficiently long guard interval (in the form of a cyclic prefix) provides intrinsic protection against IBI at the expense of extra overhead. In practical OFDM(A) applications, data transmission is organized in frames, and training blocks (carrying known symbols) are located at the beginning of each frame for synchronization purposes. On one hand, the training blocks usually have a long cyclic prefix (CP) that comprises both the channel delay spread and the propagation delay [1], [2]. On the other hand, the CP of data blocks should be made just greater than the CIR length to minimize the system overhead. Thus, accurate estimation of timing offsets in the uplink training period is desired so that we can align all users in time and avoid IBI over the data section of the frame. Finally, estimating the channel response of each user is indispensable for coherent detection of transmitted data. The above synchronization and channel estimation tasks are particularly challenging in the uplink of an OFDMA system where each user has his/her own CFO, timing error, and channel response.

Frequency and timing estimation for OFDMA uplink applications has recently received some attention and several solutions are now available. For example, the method proposed in [3] exploits redundancy offered by the CP while frequency and timing estimates are computed in [4] by looking for the position of null (virtual) subcarriers within the signal bandwidth. Both methods produce excellent results. However, they are only suitable for a subband-based carrier assignment scheme (CAS), where a group of adjacent subcarriers is allocated to one user so that signals from different users can be easily separated at the BS through a filter bank. A frequency estimation scheme for OFDMA transmissions with interleaved CAS (ICAS) is described in [5]. It is a subspace approach, which exploits the periodic structure of the signals transmitted by each user. Despite their good performance, all of the above-mentioned schemes cannot be used in OFDMA systems employing generalized CAS (GCAS), where each user can select the best available subcarriers (i.e., those with the largest channel gains) [2]. Since there is no strict association between subcarriers and users, the GCAS allows dynamic resource allocation and provides more flexibility than subband-based or interleaved schemes [6]. A method for estimating the CFO and the timing offset of a new user en-
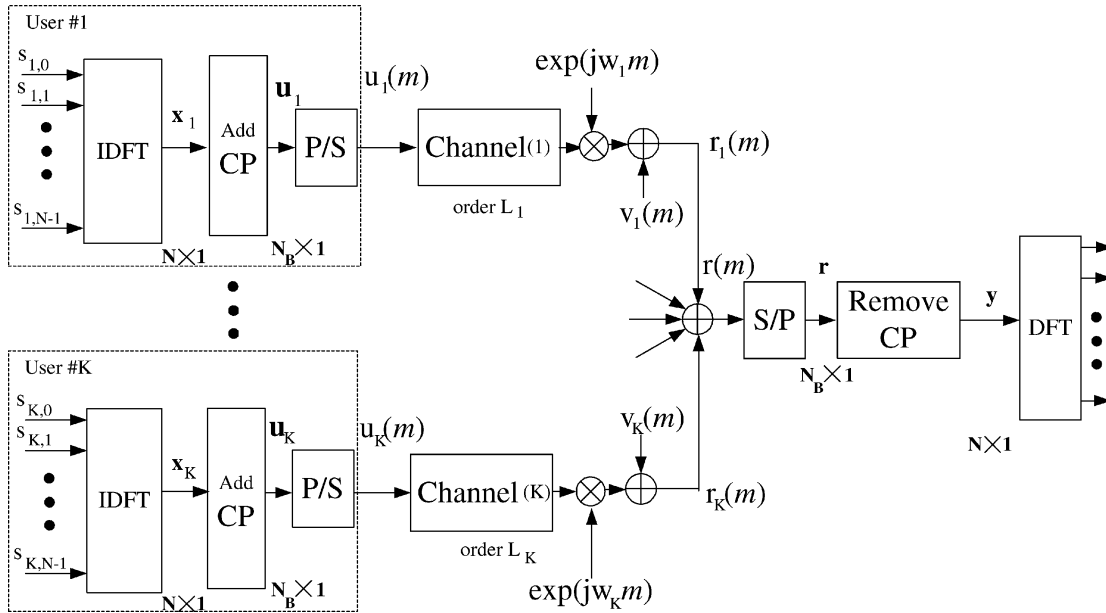
Fig. 1. Discrete-time model of the baseband OFDMA system.

tering an OFDMA system with GCAS was proposed in [7]. This scheme has good performance but assumes that all existing users have already been synchronized, which may be an issue of concern in practical applications.

In this paper, we address the problem of jointly estimating CFOs, timing offsets, and channel responses of all active users in the uplink communication of an OFDMA system. It is assumed that each user transmits a training block (carrying known symbols) at the beginning of the uplink frame. We consider a quasi-synchronous system, where the CP of a training block is sufficiently long to comprise both the channel delay spread and propagation delays incurred by users' signals. As mentioned before, in this case, accurate timing estimation is used to reduce the length of the CP during the data section of the frame. The exact maximum-likelihood (ML) solution to this problem is prohibitively complex since it demands a search over a multidimensional space. To overcome this difficulty, we resort to the alternating-projection algorithm [8] and propose a simpler scheme, in which CFOs are estimated *sequentially* instead of *jointly*. This reduces the multidimensional search problem to a sequence of simple one-dimensional (1-D) searches. The CFO estimates are then exploited to recover both the timing offset and the channel response of each user. The resulting scheme is suitable for any CAS and can be used in all practical communication systems, including IEEE802.16, where each user selects the best subcarriers in a decreasing order of channel gains. This advantage is achieved at the price of a higher computational complexity as compared to methods in [3]–[5]. The need for a training block at the beginning of each frame also leads to an increased system overhead. However, this should not be a serious concern since training blocks are specified in the frame structure of many standardized multicarrier systems [2].

The remainder of this paper is organized as follows. Section II presents the signal model for OFDMA uplink transmissions. We propose a method for estimating the CFOs of all active users in

Section III and address the problem of timing and channel estimation in Section IV. The Cramer–Rao bound (CRB) is derived in Section V to characterize the accuracy of frequency estimates. Simulation results are given in Section VI, and, finally, some conclusions are drawn in Section VII.

II. SIGNAL MODELS FOR OFDMA UPLINK TRANSMISSIONS

We consider the uplink of an OFDMA network in which K active users simultaneously communicate with the BS as depicted in Fig. 1. We use N to denote the total number of subcarriers and $\boldsymbol{s}_k(n)$ the nth block of frequency-domain symbols sent by the kth user, where $k \in \{1, 2, \cdots, K\}$. In the sequel to this study, we concentrate on a single block and omit the temporal index n for notational simplicity. The jth entry of $\boldsymbol{s}_k$, say $s_{k,j}$, is nonzero if and only if the jth subcarrier is modulated by the kth user, with $j \in \{0, 1, \cdots, N - 1\}$. This means that $\boldsymbol{s}_k$ has only N_k nonzero elements, where N_k is the number of subcarriers assigned to the kth user. The corresponding time-domain vector is given by

$$\boldsymbol{x}_k = \boldsymbol{F}^H \boldsymbol{s}_k \qquad (1)$$

where $\boldsymbol{F}$ is the N-point discrete Fourier transform (DFT) matrix with entries $[\boldsymbol{F}]_{n,k} = (1/\sqrt{N}) \exp((-j2\pi nk)/N)$ for $0 \leq n$, $k \leq N - 1$, and the superscript $(\cdot)^H$ denotes the Hermitian transpose. A CP of length N_g is appended in front of $\boldsymbol{x}_k$ to eliminate IBI. The resulting vector $\boldsymbol{u}_k$ of length $N_B = N + N_g$ is then transmitted over the channel. Calling $h_k(l)$ the discrete-time composite channel impulse response of the kth user (encompassing the transmit/receive filters and the transmission medium), the corresponding channel response vector can be written as $\boldsymbol{h}_k \stackrel{\text{def}}{=} [h_k(0), h_k(1), \cdots, h_k(L_k - 1)]^T$, where $(\cdot)^T$ is the transpose operator and L_k is the channel order. Since L_k

is usually unknown, in practice, we replace $\boldsymbol{h}_k$ by an L_h-dimensional vector

$$\boldsymbol{h}'_k \stackrel{\text{def}}{=} \begin{bmatrix} \boldsymbol{h}_k^T & \boldsymbol{0}_{(L_h-L_k)\times 1}^T \end{bmatrix}^T \tag{2}$$

where $L_h \geq \max_k \{L_k\}$ is a design parameter that depends on the duration of the transmit/receive filters and on the *maximum expected* channel delay spread.

The waveform arriving at the BS is given by the superposition of the signals from all active users. In the presence of both CFOs and timing errors, the discrete-time output of the BS receive filter is given by

$$r(m) = \sum_{k=1}^{K} \left\{ e^{j\omega_k m} \sum_{l=0}^{L_h-1} h_k(l) u_k(m-l-\mu_k) \right\} + v(m) \tag{3}$$

where

ω_k $= 2\pi \Delta f_k/N$, where Δf_k is the kth CFO normalized to the subcarrier spacing;

μ_k is the timing error of the kth user expressed in sampling intervals (as done in [7], the fractional part of the timing error is incorporated into the channel impulse response);

$v(m)$ is the noise contribution and it is modeled as a circularly symmetric white Gaussian process with variance $\sigma_v^2 = 2N_0$, where $N_0/2$ is the two-sided power spectral density of the thermal noise.

Samples $r(m)$ are divided into adjacent segments of length N_B, each corresponding to a received OFDMA block in the BS time reference. As shown in Fig. 1, the samples belonging to a given block are serial-to-parallel (S/P) converted to form $\boldsymbol{r}$. Next, the cyclic prefix is removed and the remaining samples are collected into the N-dimensional vector $\boldsymbol{y}$. We consider a quasi-synchronous system where each user achieves timing acquisition through a downlink synchronization channel before initiating the uplink transmission [7]. In this way, the timing errors in the uplink are only due to the (two-way) line-of-sight propagation delay and are limited to $\mu_{\max} = 2R/c$, where R is the cell radius and c is the speed of light. The OFDMA blocks are organized in frames and each user transmits pilot symbols over its preassigned subcarriers during a training block located at the beginning of each frame (corresponding to $n = 0$). In the following, we concentrate on the training block and let $N_g \geq L_h + \mu_{\max}$, so that vector $\boldsymbol{y}$ is not affected by IBI (as mentioned earlier, this assumption is not restrictive since training blocks are usually preceded by long CPs in practical applications). Then, from (3), it follows that $\boldsymbol{y}$ can be written as

$$\boldsymbol{y} = \sum_{k=1}^{K} \boldsymbol{\Gamma}(\omega_k) \boldsymbol{A}_k \boldsymbol{\xi}_k + \boldsymbol{v} \tag{4}$$

or equivalently

$$\boldsymbol{y} = \sum_{k=1}^{K} \boldsymbol{\Gamma}(\omega_k) \mathbf{D}_k(\mu_k) \boldsymbol{h}'_k + \boldsymbol{v} \tag{5}$$

where we have defined the following quantities:

$$\bar{\boldsymbol{\Gamma}}(\omega_k) = \text{diag} \left\{ e^{j\omega_k N_g}, e^{j\omega_k(N_g+1)} \dots, e^{j\omega_k(N_g+N-1)} \right\} \tag{6}$$

$$[\boldsymbol{A}_k]_{p,q} = [\boldsymbol{x}_k]_{|p-q|_N}, \quad 1 \leq p \leq N, 1 \leq q \leq N_g \tag{7}$$

$$\boldsymbol{\xi}_k \stackrel{\text{def}}{=} \begin{bmatrix} \boldsymbol{0}_{\mu_k \times 1}^T & \boldsymbol{h}'^T_k & \boldsymbol{0}_{(N_g-\mu_k-L_h)\times 1}^T \end{bmatrix}^T \tag{8}$$

$$[\mathbf{D}_k(\mu_k)]_{p,q} = [\boldsymbol{x}_k]_{|p-q-\mu_k|_N}, \quad 1 \leq p \leq N, 1 \leq q \leq L_h. \tag{9}$$

In the above equations, $[\boldsymbol{x}_k]_l$ denotes the lth entry of $\boldsymbol{x}_k$ for $0 \leq l \leq N-1$, and the modulo-N operation $|i|_N$ means that i is reduced to the interval $[0, N-1]$.

The major difference between (4) and (5) lies in the way the timing errors μ_k's appear in the signal model. In the first case, μ_k is embedded into $\boldsymbol{\xi}_k$, while in (5) it is incorporated into $\mathbf{D}_k$. Since we are interested in the estimation of ω_k, μ_k, and $\boldsymbol{h}'_k$ for each active user, in principle, we could exploit the signal model in (5) to jointly estimate $\boldsymbol{\omega} = [\omega_1, \omega_2, \cdots, \omega_K]^T$, $\boldsymbol{\mu} = [\mu_1, \mu_2, \cdots, \mu_K]^T$, and $\boldsymbol{h}' = [\boldsymbol{h}_1'^T, \boldsymbol{h}_2'^T, \cdots, \boldsymbol{h}_K'^T]^T$ by means of ML reasoning. This approach, however, would lead to a complex optimization problem over the $2K$-dimensional space spanned by $(\boldsymbol{\omega}, \boldsymbol{\mu})$. In an attempt to reduce the system complexity, in the following, we first use the signal model in (4) to perform joint ML estimation of $\boldsymbol{\omega}$ and $\boldsymbol{\xi} = [\boldsymbol{\xi}_1^T, \boldsymbol{\xi}_2^T, \cdots, \boldsymbol{\xi}_K^T]^T$. After obtaining the CFO estimates, the model in (5) is exploited to estimate $\boldsymbol{\mu}$ and $\boldsymbol{h}'$. In this way the estimation of the CFOs is decoupled from the estimation of the timing errors and the original optimization problem is split into two simpler optimizations over the K-dimensional domains spanned by $\boldsymbol{\omega}$ and $\boldsymbol{\mu}$. Note that, in our scheme, timing estimation is performed *after* CFO recovery while in conventional OFDM systems it typically precedes the frequency estimation task. As discussed previously, this is possible since we are considering a quasi-synchronous network where timing errors in the uplink are relatively small and a long CP is appended in front of the training block. In this respect, the estimation of $\boldsymbol{\mu}$ in the uplink can be seen as a *fine* timing adjustment that only serves to reduce the length of the CP during the data section of the frame.

III. CFO ESTIMATION

A. ML Estimation

We begin by rewriting (4) into the following equivalent form:

$$\boldsymbol{y} = \boldsymbol{Q}(\omega)\boldsymbol{\xi} + \boldsymbol{v} \tag{10}$$

where

$$\boldsymbol{Q}(\omega) = [\boldsymbol{\Gamma}(\omega_1)\boldsymbol{A}_1, \boldsymbol{\Gamma}(\omega_2)\boldsymbol{A}_2, \dots, \boldsymbol{\Gamma}(\omega_K)\boldsymbol{A}_K]. \tag{11}$$

Recalling that the entries of $\boldsymbol{v}$ are independent Gaussian random variables with zero mean and variance σ_v^2, the log-likelihood function for the unknown parameters $\boldsymbol{\omega}$ and $\boldsymbol{\xi}$ takes the form

$$\Lambda(\tilde{\boldsymbol{\omega}}, \tilde{\boldsymbol{\xi}}) = -N \ln(\pi\sigma_v^2) - \frac{1}{\sigma_v^2} \left\| \boldsymbol{y} - \boldsymbol{Q}(\tilde{\boldsymbol{\omega}})\tilde{\boldsymbol{\xi}} \right\|^2 \tag{12}$$

where $\tilde{\boldsymbol{\omega}}$ and $\tilde{\boldsymbol{\xi}}$ are trial values of $\boldsymbol{\omega}$ and $\boldsymbol{\xi}$, respectively, while $\|\boldsymbol{x}\|$ is the Euclidean norm of the enclosed vector $\boldsymbol{x}$. The joint ML

estimates of $\boldsymbol{\omega}$ and $\boldsymbol{\xi}$ are obtained by searching for the maximum of $\Lambda(\tilde{\boldsymbol{\omega}}, \tilde{\boldsymbol{\xi}})$. To do so, we keep $\tilde{\boldsymbol{\omega}}$ fixed and let $\tilde{\boldsymbol{\xi}}$ vary in the $2KN_g$-dimensional space C^{KN_g}. Then, we see that $\Lambda(\tilde{\boldsymbol{\omega}}, \tilde{\boldsymbol{\xi}})$ is maximum when

$$\hat{\boldsymbol{\xi}}(\tilde{\boldsymbol{\omega}}) = \left[\boldsymbol{Q}^H(\tilde{\boldsymbol{\omega}})\boldsymbol{Q}(\tilde{\boldsymbol{\omega}}) \right]^{-1} \boldsymbol{Q}^H(\tilde{\boldsymbol{\omega}})\boldsymbol{y}. \tag{13}$$

Next, substituting (13) back into (12) and maximizing with respect to $\tilde{\boldsymbol{\omega}}$, we obtain

$$\hat{\boldsymbol{\omega}} = \arg\max_{\tilde{\boldsymbol{\omega}}} \left\{ \|\boldsymbol{P}_{\boldsymbol{Q}}(\tilde{\boldsymbol{\omega}})\boldsymbol{y}\|^2 \right\} \tag{14}$$

where $\boldsymbol{P}_{\boldsymbol{Q}}(\tilde{\boldsymbol{\omega}}) = \boldsymbol{Q}(\tilde{\boldsymbol{\omega}})[\boldsymbol{Q}^H(\tilde{\boldsymbol{\omega}})\boldsymbol{Q}(\tilde{\boldsymbol{\omega}})]^{-1}\boldsymbol{Q}^H(\tilde{\boldsymbol{\omega}})$.

The following remarks are of interest.

1) It is shown in the Appendix that a necessary condition for the existence of $[\boldsymbol{Q}^H(\tilde{\boldsymbol{\omega}})\boldsymbol{Q}(\tilde{\boldsymbol{\omega}})]^{-1}$ is that $N_k \geq N_g$ for all users. Since $\sum_{k=1}^{K} N_k \leq N$, we conclude that the maximum number of users that the system can support is $K_{\max} = \text{int}(N/N_g)$, where $\text{int}(x)$ is the integer part of x. It is also clear that $\boldsymbol{P}_{\boldsymbol{Q}}(\tilde{\boldsymbol{\omega}})$ reduces to the identity matrix when $KN_g = N$, since, in that case, $\boldsymbol{Q}(\tilde{\boldsymbol{\omega}}) \in C^{N \times KN_g}$ is a square matrix and, accordingly, $[\boldsymbol{Q}^H(\tilde{\boldsymbol{\omega}})\boldsymbol{Q}(\tilde{\boldsymbol{\omega}})]^{-1} = \boldsymbol{Q}^{-1}(\tilde{\boldsymbol{\omega}})[\boldsymbol{Q}^H(\tilde{\boldsymbol{\omega}})]^{-1}$. Under these circumstances, $\|\boldsymbol{P}_{\boldsymbol{Q}}(\tilde{\boldsymbol{\omega}})\boldsymbol{y}\|^2$ becomes independent of $\tilde{\boldsymbol{\omega}}$ and the CFOs cannot be estimated. In summary, it follows from the above discussion that $N_k \geq N_g$ and $K < N/N_g$ are *necessary* conditions for the joint ML estimation of $\boldsymbol{\omega}$ and $\boldsymbol{\xi}$.

2) The maximization in (14) requires a grid-search over the multidimensional domain spanned by $\tilde{\boldsymbol{\omega}}$, which may be too cumbersome in practice. A viable method to reduce the system complexity consists of separating the users' signals at the BS before estimating their CFOs. This approach has been adopted in [3], [4], where users' separation is accomplished by means of a filter bank assuming that a group of adjacent subcarriers are assigned to each user (subband CAS). Alternatively, the subspace-based method in [5] can be used in conjunction with ICAS to estimate all of the CFOs through a mono-dimensional search. The above schemes are much simpler than the ML solution in (14) but, unfortunately, they are not suited for GCAS. Intuitively, we expect that the synchronization task may be somewhat complicated by GCAS. However, it is likely that this technique will be widely used in future wireless transmissions due to its potential advantages in terms of dynamic resource allocation among the active users. In this respect, it makes sense to look for synchronization schemes of affordable complexity and suited for GCAS. In the following, we address this problem and propose a solution based on alternating projection techniques. In this way, the multidimensional maximization problem in (14) is split into a series of simpler 1-D searches. The resulting scheme operates in an iterative fashion and can be used with any CAS.

B. Iterative Estimation via Alternating Projection

The alternating projection algorithm [8] is an iterative method for the solution of a multidimensional optimization problem. As mentioned previously, this technique is now exploited to reduce the K-dimensional maximization in (14) into a series of 1-D maximization problems. The resulting procedure consists of *cycles* and *steps*. A cycle is made of K steps, and each step updates the CFO of a single user while keeping the other CFOs constant at their most updated values. Without loss of generality, we follow the natural ordering $k = 1, 2, \cdots, K$ in updating the users' CFOs. Also, we denote $\hat{\omega}_k^{(i)}$ the estimate of ω_k at the ith cycle and define the $(K-1)$-dimensional vector $\hat{\boldsymbol{\omega}}_k^{(i)}$ as

$$\hat{\boldsymbol{\omega}}_k^{(i)} \stackrel{\text{def}}{=} \left[\hat{\omega}_1^{(i+1)}, \cdots, \hat{\omega}_{k-1}^{(i+1)}, \hat{\omega}_{k+1}^{(i)}, \cdots, \hat{\omega}_K^{(i)} \right]^T. \tag{15}$$

At the kth step of the $(i+1)$th cycle, the alternating projection algorithm updates the estimate of ω_k by solving the following 1-D maximization problem:

$$\hat{\omega}_k^{(i+1)} = \arg\max_{\tilde{\omega}_k} \left\{ \left\| \boldsymbol{P}_{\boldsymbol{Q}}\left(\tilde{\omega}_k, \hat{\boldsymbol{\omega}}_k^{(i)} \right) \boldsymbol{y} \right\|^2 \right\} \tag{16}$$

where $\boldsymbol{P}_{\boldsymbol{Q}}(\tilde{\omega}_k, \hat{\boldsymbol{\omega}}_k^{(i)})$ is used to indicate the functional dependence of $\boldsymbol{P}_{\boldsymbol{Q}}$ on $[\hat{\omega}_1^{(i+1)}, \cdots, \hat{\omega}_{k-1}^{(i+1)}, \tilde{\omega}_k, \hat{\omega}_{k+1}^{(i)} \cdots, \hat{\omega}_K^{(i)}]^T$. We proceed in this way until the computation of $\hat{\omega}_K^{(i+1)}$, which concludes the $(i+1)$th cycle. The results gathered so far are further refined in the $(i+2)$th cycle, where $\hat{\boldsymbol{\omega}}_k^{(i+1)}$ is employed to compute $\hat{\omega}_k^{(i+2)}$ for $k = 1, 2, \cdots, K$. Multiple cycles are performed until the CFO estimates converge to a stable solution.

Even though it is possible that the solution converges to a local maximum of $\|\boldsymbol{P}_{\boldsymbol{Q}}(\tilde{\boldsymbol{\omega}})\boldsymbol{y}\|^2$ depending on the particular initialization [8], in all of our experiments the method converged to the true CFOs in a few cycles. Two specific implementations of the alternating projection algorithm are described in the next two subsections.

C. Alternating-Projection Frequency Estimator (APFE)

In practice, the maximization problem in (16) is solved via an exhaustive grid search over the interval spanned by $\tilde{\omega}_k$. However, computing $\boldsymbol{P}_{\boldsymbol{Q}}(\tilde{\omega}_k, \hat{\boldsymbol{\omega}}_k^{(i)})$ requires a matrix inversion of order KN_g for each value of $\tilde{\omega}_k$, which may be too cumbersome for practical implementation. Fortunately, the complexity involved in the matrix inversion can be significantly reduced based on the following observations. First, we notice that most of the columns of $\boldsymbol{Q}(\tilde{\omega}_k, \hat{\boldsymbol{\omega}}_k^{(i)})$ are fixed while updating $\hat{\boldsymbol{\omega}}_k^{(i)}$. Thus, we can split $\boldsymbol{Q}(\tilde{\omega}_k, \hat{\boldsymbol{\omega}}_k^{(i)})$ into two parts: 1) $\boldsymbol{C}(\tilde{\omega}_k)$, containing all columns related to $\tilde{\omega}_k$, and 2) $\boldsymbol{B}(\hat{\boldsymbol{\omega}}_k^{(i)})$, containing all of the remaining columns of $\boldsymbol{Q}(\tilde{\omega}_k, \hat{\boldsymbol{\omega}}_k^{(i)})$ (i.e., those *not* related to $\tilde{\omega}_k$). For example, for $k = 1$, matrix $\boldsymbol{Q}(\tilde{\omega}_k, \hat{\boldsymbol{\omega}}_k^{(i)})$ can be written as

$$\boldsymbol{Q}\left(\tilde{\omega}_1, \hat{\boldsymbol{\omega}}_1^{(i)} \right) = \left[\underbrace{\boldsymbol{\Gamma}(\tilde{\omega}_1)\boldsymbol{A}_1}_{\boldsymbol{C}(\tilde{\omega}_1)}, \underbrace{\boldsymbol{\Gamma}\left(\hat{\omega}_2^{(i)} \right)\boldsymbol{A}_2, \cdots, \boldsymbol{\Gamma}\left(\hat{\omega}_K^{(i)} \right)\boldsymbol{A}_K}_{\boldsymbol{B}(\hat{\boldsymbol{\omega}}_1^{(i)})} \right]. \tag{17}$$

Next, by exploiting the special structure of $\boldsymbol{Q}(\tilde{\omega}_k, \hat{\boldsymbol{\omega}}_k^{(i)})$, we can decompose $\boldsymbol{P_Q}(\tilde{\omega}_k, \hat{\boldsymbol{\omega}}_k^{(i)})$ into two parts: 1) $\boldsymbol{P_B}(\hat{\boldsymbol{\omega}}_k^{(i)})$, which performs the orthogonal projection onto the subspace spanned by the columns of $\boldsymbol{B}(\hat{\boldsymbol{\omega}}_k^{(i)})$, and 2) $\boldsymbol{P_{C_B}}(\tilde{\omega}_k, \hat{\boldsymbol{\omega}}_k^{(i)})$, which performs the residual projection onto the subspace spanned by the columns of $\boldsymbol{C_B}(\tilde{\omega}_k, \hat{\boldsymbol{\omega}}_k^{(i)}) = (\boldsymbol{I}_N - \boldsymbol{P_B}(\hat{\boldsymbol{\omega}}_k^{(i)}))\boldsymbol{C}(\tilde{\omega}_k)$, where $\boldsymbol{I}_N$ is the identity matrix of order N. The idea behind this decomposition is similar to the Gram–Schmidt procedure, and it is mathematically expressed as

$$\boldsymbol{P_Q}\left(\tilde{\omega}_k, \hat{\boldsymbol{\omega}}_k^{(i)}\right) = \boldsymbol{P_B}\left(\hat{\boldsymbol{\omega}}_k^{(i)}\right) + \boldsymbol{P_{C_B}}\left(\tilde{\omega}_k, \hat{\boldsymbol{\omega}}_k^{(i)}\right) \qquad (18)$$

where

$$\boldsymbol{P_B}\left(\hat{\boldsymbol{\omega}}_k^{(i)}\right) = \boldsymbol{B}\left(\hat{\boldsymbol{\omega}}_k^{(i)}\right)\left[\boldsymbol{B}^H\left(\hat{\boldsymbol{\omega}}_k^{(i)}\right)\boldsymbol{B}\left(\hat{\boldsymbol{\omega}}_k^{(i)}\right)\right]^{-1}\boldsymbol{B}^H\left(\hat{\boldsymbol{\omega}}_k^{(i)}\right) \tag{19}$$

and

$$\begin{aligned}\boldsymbol{P_{C_B}}\left(\tilde{\omega}_k, \hat{\boldsymbol{\omega}}_k^{(i)}\right) =\ & \boldsymbol{C_B}\left(\tilde{\omega}_k, \hat{\boldsymbol{\omega}}_k^{(i)}\right) \\ & \times \left[\boldsymbol{C_B}^H\left(\tilde{\omega}_k, \hat{\boldsymbol{\omega}}_k^{(i)}\right)\boldsymbol{C_B}\left(\tilde{\omega}_k, \hat{\boldsymbol{\omega}}_k^{(i)}\right)\right]^{-1} \\ & \times \boldsymbol{C_B}^H\left(\tilde{\omega}_k, \hat{\boldsymbol{\omega}}_k^{(i)}\right). \end{aligned} \tag{20}$$

Since $\boldsymbol{P_B}(\hat{\boldsymbol{\omega}}_k^{(i)})$ is independent of $\tilde{\omega}_k$, we may rewrite (16) as

$$\hat{\omega}_k^{(i+1)} = \arg\max_{\tilde{\omega}_k}\left\{\left\|\boldsymbol{P_{C_B}}\left(\tilde{\omega}_k, \hat{\boldsymbol{\omega}}_k^{(i)}\right)\boldsymbol{y}\right\|^2\right\}. \tag{21}$$

Note that computing $\boldsymbol{P_{C_B}}(\tilde{\omega}_k, \hat{\boldsymbol{\omega}}_k^{(i)})$ demands the inversion of a matrix of dimension $N_g \times N_g$, which is significantly smaller than that required to compute $\boldsymbol{P_Q}(\tilde{\omega}_k, \hat{\boldsymbol{\omega}}_k^{(i)})$. In the sequel, the estimator in (21) is referred to as the APFE.

As it is intuitively clear, the APFE has a higher chance to converge to the global maximum of the likelihood function if accurate estimates $\hat{\boldsymbol{\omega}}^{(0)}$ are used for initialization. Two methods can be used to obtain $\hat{\boldsymbol{\omega}}^{(0)}$. The first possibility consists of simply initializing the CFO estimate with the expected value of ω_k, i.e., $\hat{\omega}_k^{(0)} = 0$, since ω_k is typically modeled as a zero-mean random variable. Alternatively, $\hat{\omega}_k^{(0)}$ can be taken as the output of the frequency estimator proposed in [9]. Note that the scheme in [9] was originally developed for a single-user system and, accordingly, it is not resistant to multiple-access interference (MAI). However, simulations indicate that it provides better initialization values and results in a faster convergence rate than simply setting $\hat{\omega}_k^{(0)} = 0$.

D. Approximate APFE (AAPFE)

Inspection of (20) reveals that computing $\boldsymbol{P_{C_B}}(\tilde{\omega}_k, \hat{\boldsymbol{\omega}}_k^{(i)})$ still requires a matrix inversion of dimension $N_g \times N_g$ for each value of $\tilde{\omega}_k$. Since $\boldsymbol{C}^H(\tilde{\omega}_k)\boldsymbol{C}(\tilde{\omega}_k) = \boldsymbol{A}_k^H\boldsymbol{A}_k$ is independent of $\tilde{\omega}_k$, we

can approximate the quantity $\|\boldsymbol{P_{C_B}}(\tilde{\omega}_k, \hat{\boldsymbol{\omega}}_k^{(i)})\boldsymbol{y}\|^2$ using the von Neumann series truncated to the Mth order term [10], i.e.,

$$\begin{aligned}\left\|\boldsymbol{P_{C_B}}\left(\tilde{\omega}_k, \hat{\boldsymbol{\omega}}_k^{(i)}\right)\boldsymbol{y}\right\|^2 \approx\ & \boldsymbol{y}^H\boldsymbol{C_B}\left(\tilde{\omega}_k, \hat{\boldsymbol{\omega}}_k^{(i)}\right) \\ & \times \left[\sum_{i=0}^M\left(\boldsymbol{E}\left(\tilde{\omega}_k, \hat{\boldsymbol{\omega}}_k^{(i)}\right)\right)^i\right] \\ & \times \left(\boldsymbol{A}_k^H\boldsymbol{A}_k\right)^{-1}\boldsymbol{C_B}^H\left(\tilde{\omega}_k, \hat{\boldsymbol{\omega}}_k^{(i)}\right)\boldsymbol{y} \end{aligned} \tag{22}$$

where

$$\boldsymbol{E}\left(\tilde{\omega}_k, \hat{\boldsymbol{\omega}}_k^{(i)}\right) = \left(\boldsymbol{A}_k^H\boldsymbol{A}_k\right)^{-1}\boldsymbol{C}^H(\tilde{\omega}_k)\boldsymbol{P_B}\left(\hat{\boldsymbol{\omega}}_k^{(i)}\right)\boldsymbol{C}(\tilde{\omega}_k). \tag{23}$$

Note that computing the right-hand-side (rhs) of (22) requires the inversion of $\boldsymbol{A}_k^H\boldsymbol{A}_k$, which is independent of $\tilde{\omega}_k$. This leads to a significant reduction of the system complexity, since we only need one matrix inversion for each user, irrespective of the cycle number, while APFE requires a new matrix inversion for each value of $\tilde{\omega}_k$ at each cycle. The estimator based on (22) is called the AAPFE. The initialization of AAPFE can be done exactly in the same way as for APFE.

IV. ESTIMATION OF THE TIMING OFFSETS AND CHANNEL RESPONSES

As mentioned earlier, in practical OFDMA systems, the training blocks have a long CP that comprises both the channel response duration and the two-way propagation delay to prevent IBI. On the other hand, it is desirable that data blocks have a shorter CP (of the order of the channel response duration) to reduce unnecessary overhead. For example, in the IEEE802.16a standard, the CP during the training period is two times longer than that of data blocks [1], [2]. Under these circumstances, users' signals arriving at the BS must be properly aligned in time to avoid IBI over the data section of the frame. As discussed in [7], timing and frequency compensation cannot be accomplished at the BS, as the correction of one user's offsets would misalign the other users. In practice, the BS computes the frequency and timing estimates, which are then returned back on a downlink control channel and exploited by the users to adjust their transmitter clock and carrier frequency.

The goal of this section is the joint estimation of the timing errors $\boldsymbol{\mu} = [\mu_1, \mu_2, \cdots, \mu_K]^T$ and channel responses $\boldsymbol{h}' = [\boldsymbol{h}_1'^T, \boldsymbol{h}_2'^T, \cdots, \boldsymbol{h}_K'^T]^T$ of all active users. To this end, we resort to an ML-based scheme and exploit the CFO estimate $\hat{\boldsymbol{\omega}}$ provided by either APFE or AAPFE. We begin by rewriting (5) as

$$\boldsymbol{y} = \boldsymbol{G}(\boldsymbol{\omega}, \boldsymbol{\mu})\boldsymbol{h}' + \boldsymbol{v} \tag{24}$$

where

$$\boldsymbol{G}(\boldsymbol{\omega}, \boldsymbol{\mu}) = [\boldsymbol{\Gamma}(\omega_1)\boldsymbol{D}_1(\mu_1) \quad \boldsymbol{\Gamma}(\omega_2)\boldsymbol{D}_2(\mu_2) \quad \cdots \\ \boldsymbol{\Gamma}(\omega_K)\boldsymbol{D}_K(\mu_K)]. \tag{25}$$

If the frequency offsets $\boldsymbol{\omega}$ were perfectly known, from (24), it follows that the ML estimates of $\boldsymbol{\mu}$ and $\boldsymbol{h}'$ could be obtained by searching for the minimum of

$$\Pi(\tilde{\boldsymbol{\mu}}, \tilde{\boldsymbol{h}}') = \left\| \boldsymbol{y} - \boldsymbol{G}(\boldsymbol{\omega}, \tilde{\boldsymbol{\mu}})\tilde{\boldsymbol{h}}' \right\|^2 \qquad (26)$$

with respect to $\tilde{\boldsymbol{\mu}}$ and $\tilde{\boldsymbol{h}}'$. In practice, $\boldsymbol{\omega}$ is unknown, and we can replace it by its estimate $\hat{\boldsymbol{\omega}}$. In other words, $\boldsymbol{G}(\boldsymbol{\omega}, \tilde{\boldsymbol{\mu}})$ in (26) is replaced by $\boldsymbol{G}(\hat{\boldsymbol{\omega}}, \tilde{\boldsymbol{\mu}})$.

To proceed further, we first minimize $\Pi(\tilde{\boldsymbol{\mu}}, \tilde{\boldsymbol{h}}')$ with respect to $\tilde{\boldsymbol{h}}'$, which leads to

$$\hat{\boldsymbol{h}}'(\hat{\boldsymbol{\omega}}, \tilde{\boldsymbol{\mu}}) = \left[\boldsymbol{G}^H(\hat{\boldsymbol{\omega}}, \tilde{\boldsymbol{\mu}})\boldsymbol{G}(\hat{\boldsymbol{\omega}}, \tilde{\boldsymbol{\mu}}) \right]^{-1} \boldsymbol{G}^H(\hat{\boldsymbol{\omega}}, \tilde{\boldsymbol{\mu}})\boldsymbol{y}. \qquad (27)$$

Then, substituting (27) back into (26) and minimizing with respect to $\tilde{\boldsymbol{\mu}}$, we obtain

$$\hat{\boldsymbol{\mu}} = \arg\max_{\tilde{\boldsymbol{\mu}}} \left\{ \|\boldsymbol{P_G}(\hat{\boldsymbol{\omega}}, \tilde{\boldsymbol{\mu}})\boldsymbol{y}\|^2 \right\} \qquad (28)$$

where

$$\boldsymbol{P_G}(\hat{\boldsymbol{\omega}}, \tilde{\boldsymbol{\mu}}) = \boldsymbol{G}(\hat{\boldsymbol{\omega}}, \tilde{\boldsymbol{\mu}}) \left[\boldsymbol{G}^H(\hat{\boldsymbol{\omega}}, \tilde{\boldsymbol{\mu}})\boldsymbol{G}(\hat{\boldsymbol{\omega}}, \tilde{\boldsymbol{\mu}}) \right]^{-1} \boldsymbol{G}^H(\hat{\boldsymbol{\omega}}, \tilde{\boldsymbol{\mu}}). \qquad (29)$$

The multidimensional maximization problem in (28) can be efficiently solved by resorting to the alternating-projection technique illustrated in Section III. This results in a scheme called the alternating-projection timing estimator (APTE). Again, APTE requires an initial estimate of $\boldsymbol{\mu}$, say $\hat{\boldsymbol{\mu}}^{(0)}$. The latter can be computed as follows. First, the estimates $\hat{\boldsymbol{\xi}}_k$, $k = 1, 2, \cdots, K$, are obtained by segmenting $\hat{\boldsymbol{\xi}}$ into K blocks, each of size N_g. Then, exploiting the specific structure of $\boldsymbol{\xi}_k$ given in (8), we take $\hat{\mu}_k^{(0)}$ as the index of the first significant element of $\hat{\boldsymbol{\xi}}_k$.

After $\hat{\boldsymbol{\mu}}$ is computed using APTE, it is employed in (27) to estimate the users' channel responses as

$$\hat{\boldsymbol{h}}' = \left[\boldsymbol{G}^H(\hat{\boldsymbol{\omega}}, \hat{\boldsymbol{\mu}})\boldsymbol{G}(\hat{\boldsymbol{\omega}}, \hat{\boldsymbol{\mu}}) \right]^{-1} \boldsymbol{G}^H(\hat{\boldsymbol{\omega}}, \hat{\boldsymbol{\mu}})\boldsymbol{y}. \qquad (30)$$

V. CRB ANALYSIS

In this section, we derive the CRB for the joint estimation of $\boldsymbol{\omega}$ and $\boldsymbol{\xi}$ based on the model in (4). Let $\boldsymbol{\xi}_R$ and $\boldsymbol{\xi}_I$ be the real and imaginary parts of $\boldsymbol{\xi}$ and $\boldsymbol{\eta} \overset{\text{def}}{=} [\boldsymbol{\omega}^T, \boldsymbol{\xi}_R^T, \boldsymbol{\xi}_I^T]^T$ be the set of the unknown parameters. For simplicity, we omit the functional dependence on $\boldsymbol{\mu}$ and use $\bar{\boldsymbol{\Gamma}}_k$ as a shorthand notation for $\boldsymbol{\Gamma}(\omega_k)$ in subsequent derivations. Thus, we can rewrite (4) as

$$\boldsymbol{y} = \sum_{k=1}^{K} \boldsymbol{\Gamma}_k \boldsymbol{A}_k \boldsymbol{\xi}_k + \boldsymbol{v} \qquad (31)$$

where $\boldsymbol{v}$ is a zero-mean Gaussian vector with covariance matrix $\sigma_v^2 \boldsymbol{I}_N$. The components of the Fisher Information Matrix (FIM) $\boldsymbol{F}$ are given by

$$[\boldsymbol{F}]_{i,j} = -E \left\{ \frac{\partial^2 \ln p(\boldsymbol{y}; \boldsymbol{\eta})}{\partial \eta_i \partial \eta_j} \right\}, \qquad 1 \le i, j \le K(2N_g + 1) \qquad (32)$$

where η_l is the lth entry of $\boldsymbol{\eta}$ and $p(\boldsymbol{y}; \boldsymbol{\eta})$ is the probability density function of $\boldsymbol{y}$, which reads

$$p(\boldsymbol{y}; \boldsymbol{\eta}) = \frac{1}{(\pi\sigma_v^2)^N} \exp \left\{ -\frac{1}{\sigma_v^2} \left\| \boldsymbol{y} - \sum_{k=1}^{K} \boldsymbol{\Gamma}_k \boldsymbol{A}_k \boldsymbol{\xi}_k \right\|^2 \right\}. \qquad (33)$$

Substituting (33) into (32) yields

$$\boldsymbol{F} = \frac{2}{\sigma_v^2} \begin{bmatrix} \Re\{\boldsymbol{Z}^H \boldsymbol{Z}\} & \Im\{\boldsymbol{Z}^H \boldsymbol{Q}\} & \Re\{\boldsymbol{Z}^H \boldsymbol{Q}\} \\ -\Im\{\boldsymbol{Q}^H \boldsymbol{Z}\} & \Re\{\boldsymbol{Q}^H \boldsymbol{Q}\} & -\Im\{\boldsymbol{Q}^H \boldsymbol{Q}\} \\ \Re\{\boldsymbol{Q}^H \boldsymbol{Z}\} & \Im\{\boldsymbol{Q}^H \boldsymbol{Q}\} & \Re\{\boldsymbol{Q}^H \boldsymbol{Q}\} \end{bmatrix} \qquad (34)$$

where $\boldsymbol{Q}$ is given in (11), $\Re(\boldsymbol{x})$ and $\Im(\boldsymbol{x})$ are the real and imaginary parts of $\boldsymbol{x}$, respectively, and we have defined the following quantities:

$$\boldsymbol{Z} = [\boldsymbol{z}_1 \quad \boldsymbol{z}_2 \quad \cdots \quad \boldsymbol{z}_K] \qquad (35)$$
$$\boldsymbol{z}_k = (\boldsymbol{M} + N_g \boldsymbol{I}_N)\boldsymbol{\Gamma}_k \boldsymbol{A}_k \boldsymbol{\xi}_k \qquad (36)$$
$$\boldsymbol{M} = \text{diag}\{0, 1, \cdots, N-1\}. \qquad (37)$$

Finally, the CRB for the estimation of ω_k is given by

$$\text{CRB}(\omega_k) = [\boldsymbol{F}^{-1}]_{k,k}. \qquad (38)$$

The rhs of (38) can be rewritten in a more convenient form using arguments similar to those employed in [11]. Skipping the details, it is found that

$$\text{CRB}(\omega_k) = \frac{\sigma_v^2}{2} \left[\left(\Re \left\{ \boldsymbol{\Psi}^H \boldsymbol{\Pi}_{\boldsymbol{Q}}^{\perp} \boldsymbol{\Psi} \right\} \right)^{-1} \right]_{k,k} \qquad (39)$$

where $\boldsymbol{\Psi} = [\boldsymbol{\psi}_1 \ \boldsymbol{\psi}_2 \ \cdots \ \boldsymbol{\psi}_K]$ and $\boldsymbol{\psi}_k = \boldsymbol{M}\boldsymbol{\Gamma}_k \boldsymbol{A}_k \boldsymbol{\xi}_k$ with $k = 1, 2, \cdots, K$. Finally, since $\omega_k = 2\pi\Delta f_k/N$, we have

$$\text{CRB}(\Delta f_k) = \frac{N^2 \sigma_v^2}{8\pi^2} \left[\left(\Re \left\{ \boldsymbol{\Psi}^H \boldsymbol{\Pi}_{\boldsymbol{Q}}^{\perp} \boldsymbol{\Psi} \right\} \right)^{-1} \right]_{k,k}. \qquad (40)$$

As indicated in (40), $\text{CRB}(\Delta f_k)$ depends on the specific channel realization. Since we are interested in the average performance of the proposed CFO estimators, the rhs of (40) is numerically averaged over all channel realizations, and the result is taken as a baseline in the following section.

VI. SIMULATION RESULTS

The performance of the proposed synchronization and channel estimation algorithms has been assessed by computer

simulation and compared to the relevant CRB. Without loss of generality, only the results for user#1 are illustrated.

A. System Setup

The simulated OFDMA system has $N = 128$ subcarriers and operates in the 5-GHz frequency band. The signal bandwidth is 20 MHz, corresponding to an intercarrier spacing of 156.25 kHz. The channel response of each user is generated according to the HIPERLAN/2 channel model with eight paths ($L_k = 8$). In particular, the channel coefficients are modeled as independent and complex-valued Gaussian random variables with zero mean and an exponential power delay profile

$$E\left\{|h_k(l)|^2\right\} = \lambda_k \cdot \exp\{-l\}, \quad l = 0, 1, \cdots, 7. \quad (41)$$

The constant λ_1 is chosen such that the signal power of user#1 is normalized to unity, i.e., $E\{|H_1(n)|^2\} = 1$, where $H_1(n)$ is the channel frequency response of user#1 over the nth subcarrier and expressed as

$$H_1(n) = \sum_{l=0}^{7} h_1(l)e^{-\frac{j2\pi nl}{N}}, \qquad n = 0, 1, \cdots, 127. \quad (42)$$

Parameters λ_k (with $k \geq 2$) affect the signal-to-interference ratio (SIR), and their values are varied in the simulation to assess their impact on the system performance. Transmitted symbols belong to a quaternary phase-shift keying (QPSK) constellation. Since $E\{|H_1(n)|^2\} = 1$ and $\sigma_v^2 = N_0/2$, we have $E_b/N_0 = 1/(2\sigma_v^2)$, where E_b is the average energy per received bit. The overall instability of the transmit/receive oscillators is 10 parts per million (ppm), corresponding to a maximum CFO of 50 kHz. This is tantamount to setting $|\Delta f_k| \leq 0.32$, where Δf_k is the frequency offset normalized to the intercarrier spacing.

The cell radius is 150 m so that the (two-way) maximum propagation delay is $2R/c = 1$ μs. Since the sampling period is $T_s = 1/B = 5 \cdot 10^{-2}$ μs, the maximum of μ_k is equal to 20 and the grid search in (28) can be limited to $0 \leq \tilde{\mu}_k \leq 20$. The training blocks have a CP of length $N_g = 28$ to accommodate both the channel response duration and the maximum propagation delay. To reduce the system overhead, a shorter CP of length $N_g' = 8$ is employed during the data section of the frame. This means that IBI occurs in the data blocks if $\mu_k > 0$. To meet the constraint $N_k \geq N_g$, each user transmits data over 32 distinct subcarriers. In this way, the maximum number of users the system can support is $K_{\max} = N/N_k = 4$. Unless otherwise specified, the subcarriers are randomly assigned to each user in order to demonstrate the applicability of the proposed estimators in conjunction with any subcarrier allocation strategy.

As mentioned earlier, in our scheme, the BS performs frequency and timing *estimation*, whereas the *adjustment* of the synchronization parameters is made at the user's side based on instructions transmitted via the control channel. To take this into account, during the data section of the frame, we replace ω_k and μ_k by the corresponding residual errors $\omega_k - \hat{\omega}_k$ and $\mu_k - \hat{\mu}_k$, respectively.
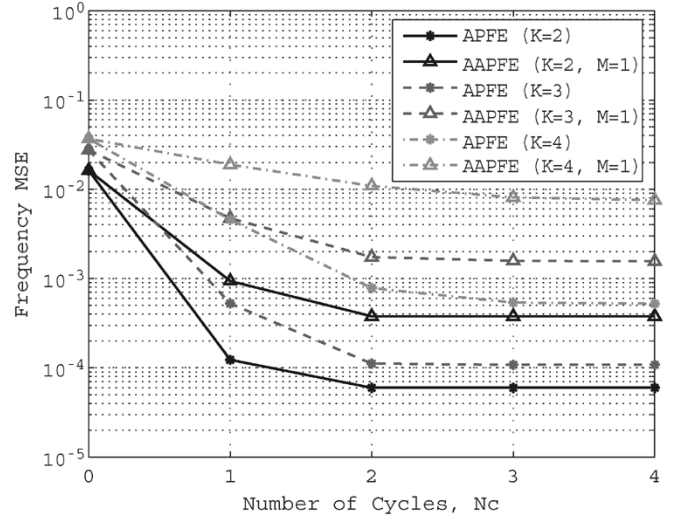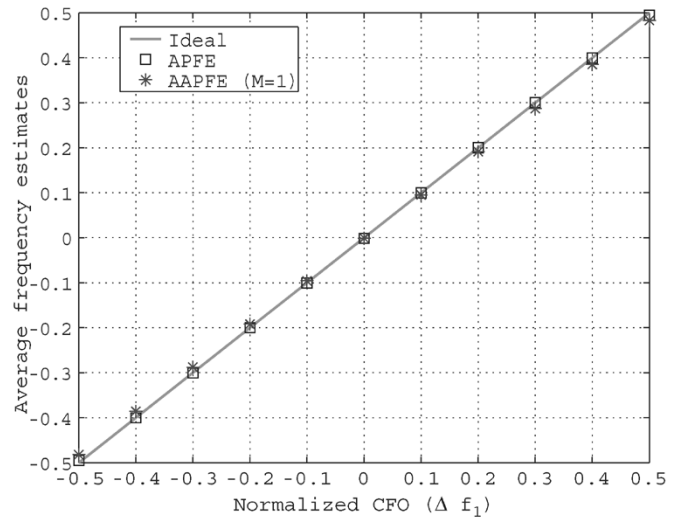

Fig. 2. Convergence rate of APFE and AAPFE.

Fig. 3. Average frequency estimates versus Δf_1.

B. Performance Assessment

Case 1: Convergence Rate and Acquisition Range of the CFO Estimators: An important design parameter for the proposed CFO estimators is the number of cycles N_c needed to achieve convergence. Fig. 2 shows the mean square error (MSE) of the normalized frequency estimates provided by APFE and AAPFE as a function of N_c for $K = 2, 3,$ and 4. All users have equal power with $E_b/N_0 = 20$ dB. The AAPFE is based on the first-order approximation of $\|P_{C_B}y\|^2$, meaning that M is set to unity in (22). The CFOs are uniformly distributed over the interval $[-0.32, 0.32]$. We see that both estimators achieve convergence in two cycles and no significant gains are observed with $N_c > 2$. For this reason, we set $N_c = 2$ in all subsequent simulations. Fig. 3 illustrates the average frequency estimates versus Δf_1 assuming that two users are active in the system. The ideal line $\mathrm{E}\{\Delta \tilde{f}_1\} = \Delta f_1$ is also drawn for comparison. We see that both APFE and AAPFE provide unbiased estimates over the range $|\Delta f_1| \leq 0.5$.
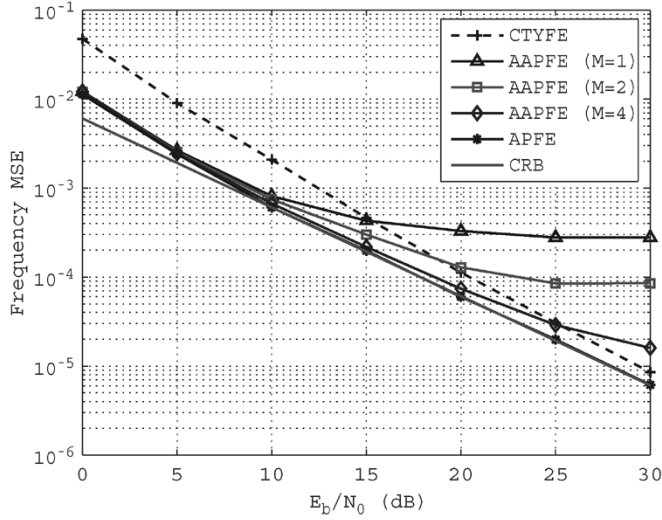
Fig. 4.   Accuracy of the various frequency estimators versus E_b/N_0.

Fig. 5.   Average IBI power versus E_b/N_0 due to timing errors.

Case 2: System Performance in the Presence of Two Users With Equal Power: In this experiment, we assess the accuracy of the proposed frequency and timing estimators in the presence of two users with equal power. Fig. 4 illustrates the frequency MSE as a function of E_b/N_0. The CRB is also shown as a benchmark. The simulation setup is the same as in Fig. 2, except that now we adopt an interleaved CAS to make comparisons with the frequency estimator proposed by Cao *et al.* (CTYFE) in [5]. We see that APFE approaches the CRB for $E_b/N_0 > 10$ dB, while AAPFE exhibits a floor that worsens as M decreases. As for CTYFE, its accuracy is satisfactory at high signal-to-noise ratios (SNRs), but significant degradations are observed with respect to APFE and AAPFE for $E_b/N_0 < 10$ dB.

The performance of the timing estimator is assessed in terms of the average IBI power due to imperfect estimates of μ_k. For a fixed error $\Delta\mu_k = \hat{\mu}_k - \mu_k$ and a channel response $\{h_k(l)\}$, the IBI power is given by [12]

$$I(\Delta\epsilon_{k,l}, \boldsymbol{h}_k) = \sum_{l=0}^{L_k-1} |h_k(l)|^2 \left[2\frac{\Delta\epsilon_{k,l}}{N} - \left(\frac{\Delta\epsilon_{k,l}}{N}\right)^2 \right] \quad (43)$$

where

$$\Delta\epsilon_{k,l} = \begin{cases} \Delta\mu_k - l, & \text{if } \Delta\mu_k > l \\ -N'_g + l - \Delta\mu_k, & \text{if } \Delta\mu_k < l - N'_g \\ 0, & \text{otherwise.} \end{cases} \quad (44)$$

Fig. 5 shows the average IBI power versus E_b/N_0 for APTE assuming ideal frequency estimation, i.e., $\hat{\omega} = \omega$. The iterations with APTE are stopped at the end of the second cycle $(N_c = 2)$.

The overall system performance has been computed in terms of uncoded bit error rate (BER). Fig. 6 illustrates the BER of a coherent QPSK system employing the proposed frequency and timing estimators. Channel estimates are computed from (30) and used to perform channel equalization according to the zero-forcing (ZF) criterion. To show the impact of the subcarrier allocation strategy on the system performance, we consider
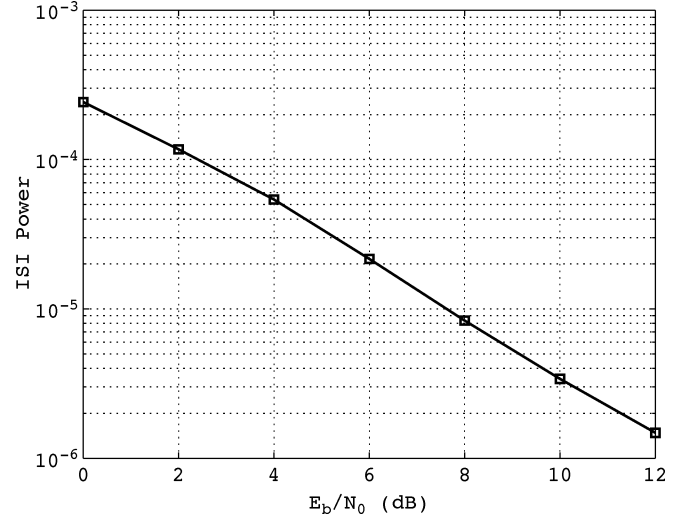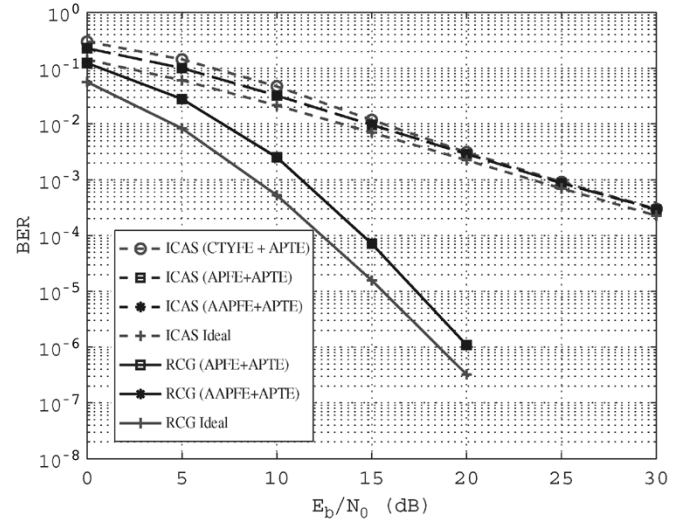

Fig. 6.   BER performance with uncoded QPSK.

two different scenarios. In the first one, we adopt an interleaved CAS (ICAS) and we use the frequency estimates provided by either APFE, CTYFE, or AAPFE (with $M = 2$). In the second scenario, the subcarriers are dynamically assigned to the active users according to the rate-craving greedy (RCG) algorithm, which was proposed in [13] to maximize the transmission rate of an OFDMA system. In the latter case, only APFE and AAPFE are considered, since CTYFE can be only used with ICAS. The curves labeled "Ideal" are obtained with perfect knowledge of the channel and synchronization parameters ($\hat{\omega} = \omega$, $\hat{\mu} = \mu$, and $\hat{\boldsymbol{h}}_k = \boldsymbol{h}_k$) and are shown as benchmarks. We see that APFE and AAPFE have similar performance, irrespective of the subcarrier allocation scheme. Results obtained with CTYFE are only marginally worse. As expected, the RCG algorithm leads to a dramatic improvement of the error rate performance as compared with ICAS. The reason for this is that dynamic subcarrier allocation provides the system with some form of *multiuser diversity* [14], which increases the asymptotic slope of the BER curves.
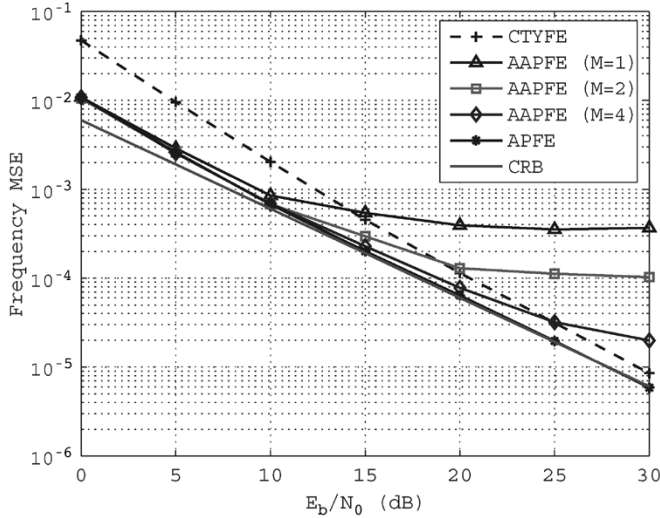
Fig. 7. Accuracy of the various frequency estimators in the presence of near–far effects.
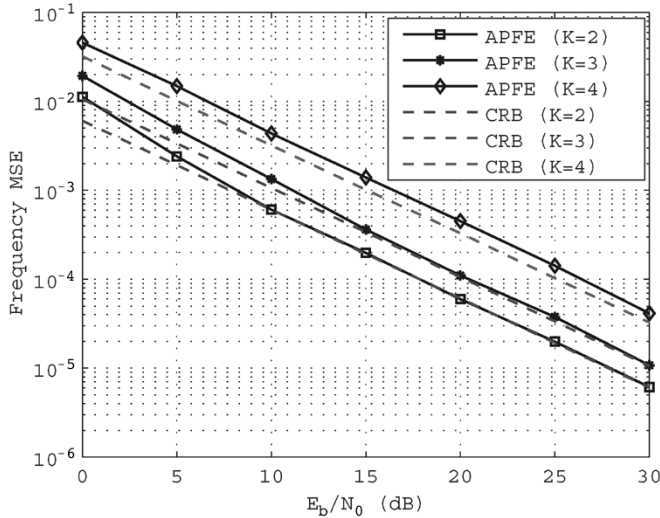

Fig. 8. Accuracy of APFE versus E_b/N_0 with $K = 2, 3,$ and 4.

Case 3: Resistance to the Near-Far Effect: Next, we investigate the resistance of the various frequency estimators to the near–far effect. For this purpose, we use the simulation setup of the previous experiment except that the power of the interfering user is now 6 dB higher than that of user#1. This can be easily achieved by setting $\lambda_2 = 4\lambda_1$ in (41). Fig. 7 shows the frequency MSE versus E_b/N_0 as obtained with APFE, CTYFE, and AAPFE (with $M = 1, 2, 4$). Comparing Figs. 4 and 7, we see that the accuracy of all of the considered schemes is only marginally affected by the near–far problem.

Case 4: Impact of K on the Accuracy of the CFO Estimates: The impact of K on the accuracy of APFE is investigated in Fig. 8, where the frequency MSE is shown as a function of E_b/N_0 for $K = 2, 3,$ and 4, assuming that all users have the same average power (i.e., $\lambda_k = \lambda_1$ for $k \geq 2$). The relevant CRBs are also shown for comparison. As expected, the estimation accuracy degrades as K grows large. In particular, the frequency MSE increases by approximately 7 dB in passing from $K = 2$ to 4. In the latter case, the MSE is 1 dB from the corresponding CRB.

C. Computational Complexity

We now assess the complexity of the proposed frequency and timing estimation schemes. We begin with the computation of the APFE metric $\|\boldsymbol{P}_{\boldsymbol{C}_{\boldsymbol{B}}}(\tilde{\omega}_k, \hat{\boldsymbol{\omega}}_k^{(i)})\boldsymbol{y}\|^2$ on the rhs of (21). From (20), we see that the crux in the calculations is the inversion of a matrix of dimensions $N_g \times N_g$, which requires approximately $\mathcal{O}(N_g^3)$ operations. Since a new metric must be computed at each cycle for all users, it follows that the complexity of APFE is $\mathcal{O}(N_g^3 K N_c N_\omega)$, where N_ω is the number of $\tilde{\omega}_k$-values over which $\|\boldsymbol{P}_{\boldsymbol{C}_{\boldsymbol{B}}}(\tilde{\omega}_k, \hat{\boldsymbol{\omega}}_k^{(i)})\boldsymbol{y}\|^2$ is evaluated. Some computational saving is possible by resorting to AAPFE. In this case, the metric is calculated as shown in (22) and (23) with approximately $\mathcal{O}(N_g N)$ operations, leading to an overall complexity $\mathcal{O}(N_g N K N_c N_\omega)$. As for APTE, it operates exactly in the same manner as APFE, except that computing the timing metric requires the inversion of a matrix of dimensions $L_h \times L_h$ rather than $N_g \times N_g$. Accordingly, the overall complexity of APTE is $\mathcal{O}(L_h^3 K N_c \mu_{\max})$, where $[0, \mu_{\max}]$ represents the uncertainty range of μ_k.

It is interesting to compare the complexity of the proposed schemes with the frequency estimator discussed in [4], which looks for the position of null subcarriers within the signal bandwidth. This requires $\mathcal{O}(N)$ operations for each user and $\tilde{\omega}_k$ value, leading to an overall complexity $\mathcal{O}(NKN_\omega)$. Recalling that $N_g = 28$ and $N_c = 2$, we see that the number of operations is approximately reduced by a factor of 56 with respect to AAPFE.

VII. CONCLUSION AND FUTURE WORK

The problem of estimating the synchronization parameters and channel responses of all active users in the uplink of an OFDMA system was investigated in this paper. The frequency estimates were obtained using an ML approach, and the alternating-projection algorithm was employed to circumvent the maximization of the likelihood function over a multidimensional space. The CFO estimates were then exploited to recover the timing errors and channel responses of the active users. Compared with other existing methods, the proposed schemes exhibit improved performance and provide more flexibility, as they can be used in conjunction with any subcarrier allocation strategy. It is fair to say that the above advantages are obtained at the price of a certain increase of the system complexity.

There are several extensions of this study that can be further explored. One possible drawback of the proposed estimators is that the maximum number of active users is constrained to be less than N/N_g. This should not represent a serious problem in wireless local area network applications characterized by small cell radii and/or channel delay spreads (leading to small values of N_g), while it can prevent their applicability to outdoor OFDMA transmissions unless the block length N is adequately increased. In practical situations, however, we can reasonably assume that only those users that are entering the system need synchronization while the others have already been frequency- and time-aligned to the BS reference. In this way, the number of unknown parameters is reduced and the constraint $K < N/N_g$ can be relaxed to $\bar{K} < N/N_g$, where $\bar{K}$ is the number of users that must be synchronized. Furthermore, throughout

the paper, only one training block has been employed for the synchronization purpose, whereas $N_T > 1$ blocks are usually available in practical systems. Multiple training blocks can be exploited in different ways. For example, they can be used to improve the estimation accuracy by averaging the frequency and timing estimates over the available blocks. Another possibility is to allocate each training block to a different group of users. Then, the system constraint can be further relaxed to $\bar{K} \leq N_T(N-1)/N_g$ and, accordingly, the maximum number of users that can enter the system at the same time is enlarged by a factor N_T. As a concluding remark, we observe that the frequency/timing estimators in [3]–[5] provide estimates of the synchronization parameters in just one OFDMA block and, accordingly, they appear to be more advantageous for outdoor transmissions than the proposed schemes. However, it should be borne in mind that the problem of channel estimation (which is indispensable for coherent data detection) is not addressed in [3]–[5]. Intuitively, we expect that this operation may require several training blocks when the delay spreads and/or cell radii are relatively large due to the huge number of parameters involved in the estimation process. In summary, although a single training block is sufficient to perform frequency and/or timing synchronization, as indicated in [3]–[5], a large overhead is still necessary in coherent outdoor transmissions to solve the channel estimation problem.

APPENDIX

Here, we discuss the invertibility of $\boldsymbol{Q}^H(\tilde{\boldsymbol{\omega}})\boldsymbol{Q}(\tilde{\boldsymbol{\omega}})$, where $\boldsymbol{Q}(\tilde{\boldsymbol{\omega}}) \in C^{N \times KN_g}$ is defined in (11). To begin with, we rewrite $\boldsymbol{Q}(\tilde{\boldsymbol{\omega}})$ as

$$\boldsymbol{Q}(\tilde{\boldsymbol{\omega}}) = [\boldsymbol{Q}_1(\tilde{\omega}_1) \quad \boldsymbol{Q}_2(\tilde{\omega}_2) \quad \cdots \quad \boldsymbol{Q}_K(\tilde{\omega}_K)] \quad (45)$$

where

$$\boldsymbol{Q}_k(\tilde{\omega}_k) = \boldsymbol{\Gamma}(\tilde{\omega}_k)\boldsymbol{A}_k, \qquad k = 1, 2, \cdots, K. \quad (46)$$

Since $\boldsymbol{\Gamma}(\tilde{\omega}_k)$ is a full-rank matrix, it follows from (46) that $\mathrm{rank}\{\boldsymbol{Q}_k(\tilde{\omega}_k)\} = \mathrm{rank}\{\boldsymbol{A}_k\}$. On the other hand, we see from (7) that $\boldsymbol{A}_k$ consists of the first N_g columns of a circulant matrix $\boldsymbol{X}_k$ with entries

$$[\boldsymbol{X}_k]_{p,q} = [\boldsymbol{x}_k]_{|p-q|_N}, \qquad 1 \leq p, q \leq N. \quad (47)$$

Using the property of circulant matrices together with (1), we have $\boldsymbol{X}_k = \boldsymbol{F}^H\boldsymbol{\Lambda}_{\boldsymbol{s}_k}\boldsymbol{F}$, where $\boldsymbol{\Lambda}_{\boldsymbol{s}_k}$ is a diagonal matrix with $\boldsymbol{s}_k$ on its main diagonal. Since $\boldsymbol{F}$ is full rank and N_k is the number of nonzero entries of $\boldsymbol{s}_k$ (i.e., the number of subcarriers assigned to the kth user), we conclude that $\mathrm{rank}\{\boldsymbol{X}_k\} = N_k$, and accordingly

$$\mathrm{rank}\{\boldsymbol{A}_k\} = \mathrm{rank}\{\boldsymbol{Q}_k(\tilde{\omega}_k)\} = \min\{N_k, N_g\}. \quad (48)$$

Now we observe that $\boldsymbol{Q}^H(\tilde{\boldsymbol{\omega}})\boldsymbol{Q}(\tilde{\boldsymbol{\omega}}) \in C^{KN_g \times KN_g}$ can be inverted if and only if $\mathrm{rank}\{\boldsymbol{Q}^H(\tilde{\boldsymbol{\omega}})\boldsymbol{Q}(\tilde{\boldsymbol{\omega}})\} = KN_g$. Using the

general results $\mathrm{rank}\{\boldsymbol{B}^H\boldsymbol{B}\} = \mathrm{rank}\{\boldsymbol{B}\}$ and $\mathrm{rank}\{[\boldsymbol{B}\,\boldsymbol{C}]\} \leq \mathrm{rank}\{\boldsymbol{B}\} + \mathrm{rank}\{\boldsymbol{C}\}$ [15, pp. 58–61], it follows from (45) and (48) that

$$\mathrm{rank}\left\{\boldsymbol{Q}^H(\tilde{\boldsymbol{\omega}})\boldsymbol{Q}(\tilde{\boldsymbol{\omega}})\right\} \leq \min\left\{N, \sum_{k=1}^{K}\min\{N_g, N_k\}\right\} \quad (49)$$

where we have taken into account that $\mathrm{rank}\{\boldsymbol{Q}(\tilde{\boldsymbol{\omega}})\}$ cannot exceed N since $\boldsymbol{Q}(\tilde{\boldsymbol{\omega}})$ has dimension $N \times KN_g$. On the other hand, since $\sum_{k=1}^{K} N_k \leq N$, we may rewrite (49) as

$$\mathrm{rank}\left\{\boldsymbol{Q}^H(\tilde{\boldsymbol{\omega}})\boldsymbol{Q}(\tilde{\boldsymbol{\omega}})\right\} \leq \sum_{k=1}^{K}\min\{N_g, N_k\}. \quad (50)$$

From the above equation, we conclude that $\mathrm{rank}\{\boldsymbol{Q}^H(\tilde{\boldsymbol{\omega}})\boldsymbol{Q}(\tilde{\boldsymbol{\omega}})\} < KN_g$ if $N_k < N_g$ for some values of k. This means that a *necessary* condition for the invertibility of $\boldsymbol{Q}^H(\tilde{\boldsymbol{\omega}})\boldsymbol{Q}(\tilde{\boldsymbol{\omega}})$ is that $N_k \geq N_g$ for $k = 1, 2, \cdots, K$.

REFERENCES

[1] G. L. Stuber, J. R. Barry, S. W. McLaughlin, Y. Li, M. A. Ingram, and T. G. Pratt, "Broadband MIMO-OFDM wireless communications," *Proc. IEEE*, vol. 92, no. 2, pp. 271–294, Feb. 2004.

[2] *IEEE Std. 802.16a Standard for Local and Metropolitan Area Networks, Part 16: Air Interface for Fixed Broadband Wireless Access Systems-Amendment 2*, IEEE Std. 802.16a, 2003.

[3] J. J. van de Beek, P. O. Borjesson, M. L. Boucheret, D. Landstrom, J. M. Arenas, O. Odling, M. Wahlqvist, and S. K. Wilson, "A time and frequency synchronization scheme for multiuser OFDM," *IEEE J. Sel. Areas Commun.*, vol. 17, no. 11, pp. 1900–1914, Nov. 1999.

[4] S. Barbarossa, M. Pompili, and G. B. Giannakis, "Channel-independent synchronization of orthogonal frequency division multiple access systems," *IEEE J. Sel. Areas Commun.*, vol. 20, no. 2, pp. 474–486, Feb. 2002.

[5] Z. Cao, U. Tureii, and Y. D. Yao, "Efficient structure-based carrier frequency offset estimation for interleaved OFDMA uplink," in *Proc. ICC*, 2003, pp. 3361–3365.

[6] C. Y. Wong, R. S. Cheng, K. B. Letaief, and R. D. Murch, "Multiuser OFDM with adaptive subcarrier, bit and power allocation," *IEEE J. Sel. Areas Commun.*, vol. 17, pp. 479–483, Oct. 1999.

[7] M. Morelli, "Timing and frequency synchronization for the uplink of an OFDMA system," *IEEE Trans. Commun.*, vol. 52, no. 2, pp. 296–306, Feb. 2004.

[8] I. Ziskind and M. Wax, "Maximum likelihood localization of multiple sources by alternating projection," *IEEE Trans. Acoust., Speech, Signal Process.*, vol. 36, no. 10, pp. 1553–1560, Oct. 1988.

[9] M. Morelli and U. Mengali, "Carrier-frequency estimation for transmissions over selective channels," *IEEE Trans. Commun.*, vol. 48, no. 9, pp. 1580–1589, Sep. 2000.

[10] D. Kincaid and W. Cheney, *Mathematics of Scientific Computing*, 2nd ed. Pacific Grove, CA: Brooks/Cole, 1996.

[11] O. Besson and P. Stoica, "On parameter estimation of/MIMO flat-fading channels with frequency offsets," *IEEE Trans. Signal Process.*, vol. 51, pp. 602–613, Mar. 2003.

[12] M. Speth, S. Fechtel, G. Fock, and H. Meyr, "Optimum receiver design for wireless broadband systems using OFDM—Part I," *IEEE Trans. Commun.*, vol. 47, pp. 1668–1677, Nov. 1999.

[13] D. Kivanc, G. Li, and H. Liu, "Computationally efficiency bandwidth allocation and power control for OFDMA," *IEEE Trans. Wireless Commun.*, vol. 2, no. 6, pp. 1150–1158, Nov. 2003.

[14] I. Li, H. Kim, Y. Lee, and Y. Kim, "A novel broadband wireless OFDMA scheme for downlink in cellular communications," in *Proc. IEEE WCNC*, Mar. 2003, vol. 3, pp. 1907–1911.

[15] H. Lutkepohl, *Handbook of Matrices*. West Sussex, U.K.: Wiley, 1996.

Man-On Pun (S'05) received the B.Eng. (Hon.) degree in electronic engineering from the Chinese University of Hong Kong in 1996, the M.Eng. degree in information sciences from the University of Tsukuba, Tsukuba, Japan, in 1999, and is currently working toward the Ph.D. degree at the Department of Electrical Engineering, University of Southern California, Los Angeles.

From 1999 to 2001, he was with the Sony Corporation, Tokyo, Japan. His current research interests are in the area of statistical signal processing for wireless communications.

Mr. Pun is a recipient of the Japanese Government (Monbusho) Scholarship and the Sir Edward Youde Memorial Fellowships for Overseas Studies.

Michele Morelli (M'04) received the Laurea (*cum laude*) degree in electrical engineering, the "Premio di Laurea SIP," and the Ph.D. degree in electrical engineering from the University of Pisa, Pisa, Italy, in 1991, 1992, and 1995, respectively.

From 1992 to 1995, he was with the Department of Information Engineering, University of Pisa. In September 1996, he joined the Centro Studi Metodi e Dispositivi per Radiotrasmissioni (CSMDR) of the Italian National Research Council (CNR), Pisa, where he held the position of Research Assistant. Since 2001, he has been with the Department of Information Engineering, University of Pisa, where he is currently an Associate Professor of telecommunications. His research interests are in wireless communication theory, with an emphasis on synchronization algorithms and channel estimation in multiple-access communication systems.

C.-C. Jay Kuo (S'83–M'86–SM'92–F'99) received the B.S. degree in electrical engineering from the National Taiwan University, Taipei, in 1980 and the M.S. and Ph.D. degrees in electrical engineering from the Massachusetts Institute of Technology, Cambridge, in 1985 and 1987, respectively.

He was Computational and Applied Mathematics (CAM) Research Assistant Professor in the Department of Mathematics, University of California, Los Angeles, from October 1987 to December 1988. Since January 1989, he has been with the Department of Electrical Engineering-Systems and the Signal and Image Processing Institute, University of Southern California, Los Angeles, where he currently has a joint appointment as Professor of Electrical Engineering and Mathematics. He has guided about 60 students to their Ph.D. degrees and supervised 15 Postdoctoral Research Fellows. He is coauthor of seven books and more than 700 technical publications in international conferences and journals. His research interests are in the areas of digital signal and image processing, audio and video coding, multimedia communication technologies and delivery protocols, and embedded system design. He is Editor-in-Chief for the *Journal of Visual Communication and Image Representation* and Editor for the *Journal of Information Science and Engineering* and the EURASIP *Journal of Applied Signal Processing*.

Dr. Kuo is a Fellow of SPIE and a member of ACM. He was on the Editorial Board of the *IEEE Signal Processing Magazine*. He served as Associate Editor for the IEEE Transactions on Image Processing from 1995 to 1998, the IEEE Transactions on Circuits and Systems for Video Technology from 1995 to 1997, and the IEEE Transactions on Speech and Audio Processing from 2001 to 2003. He was the recipient of the National Science Foundation Young Investigator Award and Presidential Faculty Fellow Award in 1992 and 1993, respectively.